HHS Public Access

Author manuscript

Metrologia. Author manuscript; available in PMC 2020 May 14.

Published in final edited form as:

Metrologia. 2018 February 28; 55(2): 254–267. doi:10.1088/1681-7575/aaa368.

Differentiating gold nanorod samples using particle size and shape distributions from transmission electron microscope images

Eric A Grulke[1], **Xiaochun Wu**[2], **Yinglu Ji**[2], **Egbert Buhr**[3], **Kazuhiro Yamamoto**[4], **Nam Woong Song**[5], **Aleksandr B Stefaniak**[6], **Diane Schwegler-Berry**[6], **Woodrow W Burchett**[7], **Joshua Lambert**[7], **Arnold J Stromberg**[7]

[1]Chemical and Materials Engineering, University of Kentucky, Lexington, KY, United States of America

[2]CAS Key Laboratory of Standardization and Measurement for Nanotechnology, CAS Center for Excellence in Nanoscience, National Center for Nanoscience and Technology, Beijing 1001901, People's Republic of China

[3]Physikalisch-Technische Bundesanstalt (PTB), Braunschweig, Germany

[4]National Institute of Advanced Industrial Science and Technology (AIST), Tsukuba, Japan

[5]Korea Research Institute of Standards and Science (KRISS), Daejeon, Republic of Korea

[6]US National Institute for Occupational Safety and Health (NIOSH), Morgantown, WV, United States of America

[7]Applied Statistics Laboratory, University of Kentucky, Lexington, KY, United States of America

Abstract

Size and shape distributions of gold nanorod samples are critical to their physico-chemical properties, especially their longitudinal surface plasmon resonance. This interlaboratory comparison study developed methods for measuring and evaluating size and shape distributions for gold nanorod samples using transmission electron microscopy (TEM) images. The objective was to determine whether two different samples, which had different performance attributes in their application, were different with respect to their size and/or shape descriptor distributions. Touching particles in the captured images were identified using a ruggedness shape descriptor. Nanorods could be distinguished from nanocubes using an elongational shape descriptor. A non-parametric statistical test showed that cumulative distributions of an elongational shape descriptor, that is, the aspect ratio, were statistically different between the two samples for all laboratories. While the scale parameters of size and shape distributions were similar for both samples, the width parameters of size and shape distributions were statistically different. This protocol fulfills an important need for a standardized approach to measure gold nanorod size and shape distributions for applications in which quantitative measurements and comparisons are important. Furthermore, the validated protocol workflow can be automated, thus providing consistent and rapid

eric.grulke@uky.edu.

Supplementary material for this article is available online

measurements of nanorod size and shape distributions for researchers, regulatory agencies, and industry.

Keywords

gold nanorod; transmission electron microscopy; size distribution; shape distribution

1. Introduction

Anisotropic metal nanoparticles, with different size, shape, and aspect ratios, have a variety of useful properties (Murphy et al 2005). Metal nanorods have shape-dependent optoelectric properties, such as surface-enhanced Raman scattering (Nikoobakht et al 2002), fluorescence (Mohamed et al 2000), and anisotropic chemical reactivity (Jana et al 2002). Apart from their high chemical stability, gold nanorods are of special interest due to their well-developed synthesis methods. These can produce nanorod samples with a wide range of tunable, longitudinal surface plasmon resonances (LSPRs), which correlate with their aspect ratios (Schmucker et al 2010, Hu et al 2014a, 2014b). Optical applications of gold nanorods include sensing and imaging based on light absorption (Murphy et al 2005), laser-induced heating (Perez-Juste et al 2005), photothermal cancer therapy (Huang et al 2007, Wang et al 2011, Alkilany et al 2012, Zhang et al 2012, 2014, Dembereldorj et al 2014), surface plasmon resonance-enhanced properties plus Raman scattering (Huang et al 2007), plasmon-induced charge separation (Du et al 2009, Kou et al 2016), drug delivery (Alkilany et al 2012, Chen et al 2016), and sensing the deformational mechanics fields of living cells (Murphy et al 2008), to name a few. Biological applications of gold nanorods are expected to increase due to their excellent biocompatibility (Huang et al 2009). Applications leading to quantitative results would benefit from size and shape distribution data with known repeatability, reproducibility, and uncertainty. Examples would be the prediction of maximum longitudinal plasmon resonance (Brioude et al 2005, Prescott and Mulvaney 2006) and the elucidation of gold nanorod growth kinetics (Henkel et al 2009) and mechanisms (Hubert et al 2010, 2012). Transmission electron microscopy (TEM) can provide high-quality data of particle size and shape distributions that can be used for process monitoring, product characterization, and other commercial applications. Despite accurate determination of gold nanorod size and shapes using TEM, the absence of a TEM measurement protocol for gold nanorod size and shape distributions hinders its technological advancement and commercial development. In this article, we report the development of a validated standardized protocol for gold nanorod size and shape distributions to meet this industrial need.

1.1. Gold nanorod sample morphologies

Gold nanorod synthesis methods can generate a variety of shapes, including rods, stars, tetrapods, blocks, and cubes (Murphy et al 2005). These morphologies are influenced by reactant concentrations, synthesis temperature and pH, and stabilizers for the seed particles (Sharma et al 2009a, Khlebtsov et al 2014). Batch, seed-mediated methods often start with 2–4 nm seed particles, and use structure-directing additives to control the nanorod

morphology during synthesis (Henkel et al 2009). The change in linear dimensions with time can be modeled as a first-order process (Henkel et al 2009).

Most seed-mediated synthesis processes also produce small number-fractions of different shaped nanoparticles (Morita et al 2009). For example, Morita and coworkers (2009) simulated the small angle x-ray scattering signal for a mixture of nanorods with an aspect ratio (defined as width divided by length, see section 1.3) of 0.33 (96.5% portion), and fat cylindrical particles with an aspect ratio of 1 (3.5% portion). The theoretical scattering profile of the mixture diverged measurably from that of the nanorod component across a range of scattering intensities. Therefore, it is likely that some commercial applications will require determination of particle size and shape distributions, and subsequent separation and removal of non-nanorods shapes from the assynthesized product (Sharma et al 2009a, 2009b, Nguyen et al 2015, 2016).

Concentrated liquid dispersions of nanorods can form liquid crystalline phases (Sharma et al 2009a). For example, phase diagrams of isotropic, nematic, smectic, and solid liquid crystallites have been computed by Bolhuis and Frenkel (1997). The phase behaviors depend on aspect ratio, the fraction of non-nanorods, the drying rates, and the polydispersities of the samples (Sharma et al 2009a). Self-association of nanorods while mounting them on TEM grids and supports can lead to touching particles that can affect automated image analysis methods. Protocols for mounting gold nanorod samples can be optimized for specific samples, depending on these and other factors.

Based on commercial synthesis techniques and applications, stakeholders for size and shape distribution measurements of gold nanorod samples may have the following needs: (1) identification of nanorod and ‘non-nanorod’ particles, (2) identification of ‘touching’ particles (linked with the formation of associating nanoparticles during the mounting protocol for TEM grids), (3) measurement of nanorod dimensions, length and width, plus their relative size distributions, and (4) the determination of nanorod aspect ratios. In addition, it would be useful to find ways to differentiate between samples having different distributions, which could directly lead to changes in their performance in applications. For instance, gold nanorod samples intended for photothermal treatments would generally have narrow size distributions that would reduce the needed laser power. For solar energy harvesting, gold nanorod samples would generally have broad size distributions for wide spectral absorbance.

1.2. Project objectives

The overall objective of the project was to determine whether two different nanorod samples, which had different performance attributes in their application, could be differentiated using size or shape descriptor distributions. The workflow to accomplish this objective included raw data triage, identification and removal of touching particles, identification and removal of non-nanorod particles, determining the repeatability and reproducibility of descriptors, non-parametric comparison of descriptors and their cumulative distributions, fitting distribution parameters to datasets and determining their uncertainties, determining whether there were fitted distribution parameters that could be used to differentiate the two samples, and visualizing the results. Touching particles were

identified using solidity, a ruggedness shape descriptor. Non-nanorod particles were identified using the aspect ratio, an elongational shape descriptor. The key size and shape descriptors used to differentiate between the two samples were Feret diameter (Feret), minimum Feret diameter (minFeret), and aspect ratio. Other descriptor choices are possible. Quantitative size and shape distributions could be linked to applications such as estimating LSPR (Brioude et al 2005, Juve et al 2013), centrifugation to separate nanorods by shape (Sharma et al 2009a, 2009b), or asymmetric flow field flow fractionation (Nguyen et al 2015, 2016) to separate nanorods by shape.

This study on gold nanorods is intended as a foundational work for a potential ISO standard on the measurement of particle size and shape distributions by TEM. It is one of five case studies undertaken as an interlaboratory comparison (ILC) project of ISO/TC229 Nanotechnologies; co-authors are members of the Joint Working Group 2 Committee, Measurement and Methods. The team includes national metrology institutes, a national center for nanoscience and technology that manufactured the samples, a US research agency, and a university.

Figure 1 shows an image of a gold nanorod sample taken by scanning electron microscopy in transmission mode. Each sample had mixtures of particle shape populations. The image shows complex touching particles, nanorods, and ‘nanocubes’, a generic term intended to include cubes, spheroidal, and other shapes with high aspect ratios (width to length ratios). The nanocubes are thought to be artefacts of the synthesis process. Notice that there are many small ‘nematic’ regions in which the nanorods are self-aligned.

1.3. Descriptor selection

We have adopted descriptor definitions as provided by ISO (2008), including those derived as ratios of size descriptors. For example, the aspect ratio is defined so that its values range from zero to one, rather than following the common convention that aspect ratios are defined as greater than or equal to one. Evaluating nanorod morphology by TEM will require at least two descriptors: for example, a size descriptor and a elongational shape descriptor (Becker et al 2010). Size descriptors used in this study were area, Feret diameter (Feret), minimum Feret diameter (minFeret), and perimeter. Elongational and ruggedness shape descriptors can be derived from combinations of size descriptors. A common set of elongational and ruggedness descriptors are shown in table SI-8 in section 7 of the supplementary information (SI) (stacks.iop.org/MET/55/254/mmedia). The aspect ratio, defined as the ratio of minFeret/Feret (ISO 2008), is often used to characterize the elongational shape of nanorods:

$$\text{aspect ratio} = \frac{\text{minFeret}}{\text{Feret}}. \quad (1)$$

In this form, low aspect ratio values correspond to long objects, while aspect ratio values near 1 correspond to spheroidal or cubical shapes. The Feret diameter and aspect ratio are often used as the two descriptors for reporting nanorod morphology. The discrete, non-touching particles in figure 1 should not have much surface ruggedness or boundary irregularities. However, ruggedness shape descriptors might be useful in identifying

touching particles, which should have significant surface ruggedness. An example of a ruggedness descriptor is solidity:

$$\text{solidity} = \frac{A}{A_C} \tag{2}$$

where A is the area of the particle, and A_C is the particle's convex hull. The area of the convex hull can be thought of as the area enclosed by a rubber band around the 2D image. For a perfect, smooth circle, the solidity should approach 1. For a highly branched image, the solidity may be much smaller than 1.

While there are predictions on how many particles must be analyzed to reliably determine the particle size and shape (Souza and Menegalli 2011) of a sample, practitioners can adjust the number of particles measured to provide parameters with the needed uncertainty (JCBM/WG1 2008). One guideline is the simple heuristic that the relative standard error of the descriptors should scale with $1/\sqrt{n}$ (Masuda and Iinoya 1970, Masuda and Gotoh 1999), where n is the number of nanoparticles measured.

1.4. Non-parametric and quantitative comparisons of descriptor datasets

Three non-parametric statistical methods were used to assess data repeatability, reproducibility, and dataset similarity: analysis of variance (ANOVA), bivariate analysis, and the two-sample Kolmogorov–Smirnov (K–S) analysis. This suite of non-parametric tests provides alternatives for comparing datasets. The ANOVA hypothesis is that there is no difference between the mean value of a descriptor for a specific dataset and the grand mean value of the descriptor for all datasets. The bivariate analysis hypothesis is that there are no differences between the mean values of two variable descriptions of a dataset, for example, a two-variable correlation or an empirical cumulative distribution. When the p-value is greater than 0.05, the null hypothesis is not rejected, and the datasets are considered similar. The K–S statistic quantifies distances between empirical cumulative distributions of two samples. The null hypothesis is that the samples are from the same distribution, testing whether the two cumulative distributions are different. The two empirical distributions are compared to find the supremum of the difference between them, $D_{n,m}$:

$$D_{n,m} = \sup\left|\left[F_{1,n}(x) - F_{2,m}(x)\right]\right| \tag{3}$$

where $F_{i,n}(x)$ is the value of the cumulative distribution of the ith sample at x, and n and m are the number of data points in each sample. Setting $1 - \alpha$ at the 95% probability level, the null hypothesis would be rejected when

$$D_{n,m} > c(\alpha) \cdot \sqrt{\frac{n+m}{n \cdot m}} \tag{4}$$

and the two empirical cumulative distributions would be considered different. At the 95% probability level, $c(\alpha) = 1.36$. The K–S test should be particularly useful for determining whether cumulative descriptor distributions of two samples are different, without reference to any particular reference model.

Quantitative comparisons of descriptor distributions are done using parameters determined by fitting reference distributions (normal, lognormal, and Weibull, for example) to empirical cumulative distributions. These models require two parameters: a distribution scale and a distribution width. Scale and width parameters can be compared across multiple datasets to generate a grand mean and a standard deviation for a specific descriptor. Uncertainties have been reported for nanoparticle size (Takahashi et al 2008, Song et al 2009, Klein et al 2011, Bell et al 2012, Nontapot et al 2013), size distributions (Braun et al 2011), surface area (Bau et al 2010), and surface topology (De Temmerman et al 2014), and are migrating from their use in characterizing reference materials (Kestens and Roebben 2014) to more routine characterizations of commercial nanoparticles.

2. Experimental details

2.1. Materials

Gold nanorod test samples were prepared using a method similar to that used to make a certified reference material (CRM Au 720, GSB 02-2994-2013 (GSB 2013)) developed by the National Center for Nanoscience and Technology (NCNST), Beijing, China. Four samples of gold nanoparticles coated with cetyltrimethylammonium bromide (CTAB), a surfactant used to stabilize water dispersion, were received from NCNST. Two particle sample types were distributed in two different states. The sample states were aqueous suspensions of gold nanoparticles and 3 mm TEM grids that were pre-loaded with nanoparticles. Sample 1 was purported to have a broader size distribution than Sample 2. Upon receipt, all samples were stored at 4 °C until use. The pre-loaded grids were used as-received.

For TEM instruments, the calibration protocols, preferred mounting methods, instrument settings, operating conditions, and image analysis methods and software can vary. An integrated protocol example, reported by one lab (L3), of the mounting method, operating conditions, and analysis of dispersion samples is provided here. Additional information about the protocol, including instrument settings, image capture, and particle analysis, is given in sections 1–5 of the SI.

2.1.1. Sample mounting.—A suspension of CTAB-coated gold nanoparticles was placed in a 30 °C water bath for 30 min to dissolve any CTAB crystals that formed during refrigeration. Next, 5 μl of the suspension was deposited onto a 300 mesh copper grid with formvar coating (Cat. No. 01701-F, Ted Pella Inc., California, USA) that was dried at ambient temperature. This sample was referred to as user-mounted. The pre-loaded grids provided by NCNST were referred to as lab-mounted.

2.1.2. Image acquisition.—Representative details of the image acquisition parameters for one laboratory are summarized in table 1. Briefly, the TEM was operated at an accelerating voltage of 80 kV and nominal magnification of 80 k. The actual magnification used for TEM image acquisition was previously calibrated using a calibration grating, although the exact date was not reported. The TEM calibration should be known and reported. Bright field images are preferred, and each image should contain a reference scale.

2.1.3. Particle capture.—Digitized images were analyzed using ImageJ version 1.49a (Schindelin et al 2015). In lab L3, the pixel size was 0.926 nm pixel^{-1} (or 1.08 pixel nm^{-1}). The brightness and contrast of each 16 bit *.tif format image was adjusted using the automatic settings optimized by ImageJ. An example of a thresholding sequence is provided in section 3 of the SI (figures SI-1–SI-4). After thresholding the images, some particles were observed to be touching. The width (minimum Feret diameter) and length (Feret diameter) were measured using the Analyze Particle function in ImageJ. The aspect ratio was computed as the ratio of the minimum Feret diameter divided by the Feret diameter. Automated algorithms for separating touching particles were not used as they can artificially reduce size and area measurements (Rice et al 2013).

2.2. Analysis workflow

2.2.1. Raw data triage and particle differentiation.—Each dataset was evaluated to determine whether touching particles and non-nanorod particles were present or had been previously removed. Nanorods were arbitrarily defined as particles with aspect ratios ⩽0.5. Differentiation criteria for touching particles and nanoparticle types were developed by one laboratory. One image was selected, and ImageJ was used to acquire and analyze each particle. Each particle was catalogued with respect to its category, i.e. nanorod, nanocube, or complex (adjacent touching particles). ANOVA was used to determine criteria for size or shape descriptors that would differentiate the three particle types (complex, nanocube, and nanorod). These criteria were translated to an automated workflow applied to all raw datasets. Touching particles were removed first, followed by nanocube data. Only nanorod data was analyzed for the remainder of the workflow (see figure SI-5).

2.2.2. Non-parametric comparisons of empirical distributions.—Two non-parametric comparison tools, ANOVA and bivariate analysis, were implemented in R Shiny App® web-based interfaces developed by the Applied Statistic Lab at the University of Kentucky. Intralaboratory repeatability can be assessed by ANOVA of descriptor means across all images for one lab. Interlaboratory reproducibility can be assessed by ANOVA of descriptor means across all datasets. Bivariate analysis compares two-variable correlations, such as size versus shape or empirical cumulative distributions, without reference to specific distribution models. These tools have been previously used for analyzing size and shape distributions of nanoparticles (Grulke *et al* 2017a, 2017b).

2.2.3. Quantitative comparison of fitted distribution parameters.—A tool for fitting normal, lognormal, and Weibull distributions to descriptor datasets was implemented in R, and linked to Shiny App web-based interfaces by the Applied Statistics Lab at the University of Kentucky. Two fitting techniques, maximum likelihood estimates and non-linear regression estimates, were used for each descriptor distribution. Scale and width parameter estimates plus their standard errors were computed for both techniques. The parameter estimates and standard errors can be used to estimate coefficients of variation and uncertainties of distribution scales and widths. The grand mean, $\bar{x}$, and its standard deviation, s, of descriptor scales and widths were computed across all datasets. The relative coefficient of variation, C_v, is the ratio of the standard deviation of the parameter values for all datasets (s) divided by the grand average of the parameter ($\bar{x}$):

$$C_v = \frac{s}{\bar{x}}. \quad (5)$$

Coefficients of variation are converted to uncertainty values for the fitted parameters (Linsinger et al 2012):

$$U_{ILC} = k \cdot C_v \cdot \sqrt{1 + 1/n} \quad (6)$$

where U_{ILC} is the uncertainty of the parameter for the ILC, k is taken as 2, and n is the number of observations. As the number of datasets, n, increases, the uncertainty decreases. Equation (6) is often used to estimate uncertainty of certified reference materials (Linsinger et al 2012). Other elements can be included in the uncertainty estimate, but only this simplified form was used for this study. Visualization tools, such as quantile plots and residual deviation plots, were used to evaluate the ranges over which models best fit the data.

3. Results

3.1. Raw data triage and image differentiation

This section addresses the triage of raw data to identify and differentiate between particle types, data repeatability, data reproducibility, and selection of descriptors for the rest of the analysis. A workflow for raw data triage is shown in figure SI-5 of the SI. Data repeatability is an important issue for analyzing particle size and shape distributions, and laboratories were encouraged to use ANOVA analysis of their data to identify whether any image-to-image bias existed. For the particles in figure 1, the aspect ratios of discrete nanorods would typically be 0.50 or less. Discrete nanorods would also have convex hull measurements, such as the convex hull of the area or the convex perimeter, similar to their total area or perimeter. This would result in ruggedness descriptors linked to their convex hulls, such as solidity or convexity, having values close to one (see table SI-8 for shape descriptor definitions). Figure 2 shows the ANOVA analysis of six images of aspect ratio data for Sample 2 reported by lab L2. The grand mean aspect ratio across all images is ~0.37 (vertical line across all boxplots). All six of these images have means (indicated by the black diamonds for each image) similar to the grand mean ($p = 0.76$), thus showing that the intralaboratory repeatability of the aspect ratio descriptor is good. However, there are a number of points, shown as asterisks, with aspect ratios greater than 0.5; these are likely to be nanocubes that should be removed from the nanorod analysis.

Figure 3 shows the ANOVA analysis of six images of solidity data for Sample 2 reported by lab L2. The grand mean solidity across all images is ~0.94 with $p = 0.076$, showing that the intralaboratory repeatability of this descriptor is good. However, there are some particles with solidities less than 0.85, which is more than two standard deviations lower than their image means. These are likely to be touching particles because the actual particle area is less than 85% of the area of its convex hull. ANOVA of image-wise data helps demonstrate intralaboratory repeatability, but can also identify the possibilities of different particle shapes and touching particles in TEM images.

3.1.1. Identification of touching particles, non-nanorods.—We have developed a heuristic method to differentiate between nanorods, nanocubes, and complex, touching particles. Using an image from one laboratory, all ImageJ-inventoried particles were cataloged with respect to being nanocubes, nanorods, or touching complexes. Figure 4 is an example of the particle outlines recovered with ImageJ: arrows point to a complex particle (1), a discrete nanorod (2), and a discrete nanocube (3). Of the 142 particles reported, 21 are complex particles that should be rejected, 11 are nanocubes that should be removed by sorting, and the remainder are nanorods. Each particle was catalogued as one of these types, and the raw data were analyzed using one-way ANOVA to determine which, if any, elongational or ruggedness shape descriptors could be used to differentiate between these image morphologies.

An ANOVA comparison of descriptor data showed that solidity, a ruggedness/boundary irregularity descriptor, provides the best differentiation between touching complexes and discrete nanoparticles such as nanocubes and nanorods. Particles with solidities less than 0.9 are characterized as touching, and particles with solidities greater than 0.9 are discrete nanorods or nanocubes. Particles with solidities less than 0.9 were removed from further analysis as their reported sizes would be much larger than discrete nanorods. Nanocubes could be separated from nanorods using the aspect ratio or ellipse ratio elongational descriptors. Based on this test case, particles with aspect ratios greater than 0.75 were characterized as nanocubes. Figure 5 is an aspect ratio versus solidity plot of the figure 4 particles. Touching particles have a broad range of the elongational descriptor, the aspect ratio, but can easily be differentiated from discrete particles using solidity. Nanorods and nanocubes have high solidities, but dissimilar ranges for aspect ratio.

This specific workflow may not generalize to a protocol that would always differentiate well between touching particles and non-touching particles for an arbitrary sample. Rather, raw data triage should probably be done on new materials tested by a laboratory in order to determine how the imaging software captures, thresholds, and reports particles; this should be followed by any appropriate revisions for the example workflow (figure SI-5). For example, particle areal density across the TEM field of view has an impact on the number of touching particles. This can be controlled via the protocol developed for the sample.

3.1.2. Selection of descriptors for nanorod morphology.—Hentschel and Paige (2003) developed a reduced set of descriptors to characterize particle shape, using both elongational and ruggedness shape descriptors. In this case, a ruggedness shape descriptor, solidity, can differentiate between complex and discrete particles; meanwhile, an elongational shape descriptor, the aspect ratio, can differentiate between nanorods and nanocubes. Because not all laboratories reported ruggedness descriptors, ranges of compactness and the aspect ratio that would correspond to solidities greater than 0.90 were used to identify touching, complex particles. Then, the aspect ratio was used to differentiate between nanocubes ($0.75 < \text{aspect ratio} < 0.9$) and nanorods ($0.20 < \text{aspect ratio} < 0.50$). The removal of nanocubes from the datasets was essential toward achieving high-quality descriptor distributions that could be fitted by unimodal models. The application of this heuristic to all datasets resulted in the removal of ~3.4% of the reported particles. About

0.4% of the reported particles appeared to be complex (touching particles), and 3% of the reported particles were nanocubes.

Commercial nanoparticle samples often contain artefacts, contaminants, and/or byproduct particles. ANOVA analysis and distribution plots can help identify the presence of significant fractions of particles with different and/or unwanted morphologies. Another common challenge for imaging samples is their self-association on TEM supports. ANOVA analysis and data visualization of different descriptors of cataloged images can help identify which descriptor ranges appear to be unique for touching particles. For gold nanorods, touching particles need to be removed from the discrete particles for consistent results.

3.2. Data repeatability and reproducibility

Many standards stakeholders, i.e. industry, regulatory, metrology, and academic, will need analysis workflows that evaluate temporal reproducibility of size and shape distributions for nanomaterials. ANOVA analysis can be used to determine whether descriptor means of datasets are similar. Bivariate analyses (Szekely and Rizzo 2004, Rizzo and Szekely 2016) can determine whether distribution data are similar; these represent more rigorous statistical tests. However, neither of these methods provide parameter estimates of reference models, which can be used to estimate coefficients of variation or uncertainties. Additional analysis of data repeatability and reproducibility is provided in sections 5 and 6 of the SI.

3.3. Non-parametric comparison of two samples

3.3.1. ANOVA comparison.—Table 2 shows ANOVA *p*-values for the pair-wise comparison of the two samples for labs L1–L5. Lab L6 was not included because its data dominates the grand average due to its large number of points. Labs 1–5 reported between 482 to 840 particles that could be evaluated, while lab 6 reported 6406 particles that could be evaluated. For two size and two shape descriptors, the scale parameters are shown to be similar but the width parameters are shown to not be similar. These results suggest that descriptor distribution widths may be different. The bivariate analysis tests can also be used to demonstrate whether datasets are similar; additional information is provided in section 6 of the SI.

3.3.2. K–S two-sample test.—The K–S two-sample test can compare two empirical distributions, returning a statistic that indicates whether they are different. Applying this test to the Sample 1 and 2 aspect ratio distributions for each lab can determine whether the data are different without referring to any specific model. Intralaboratory comparisons of the two samples avoid issues of instrument calibration and imaging thresholding, assuming that similar operators and instrumentation were used for both samples. An example of the application of the K–S two-sample method to one dataset is given in the SI. Figure 6 shows the differences between the two cumulative aspect ratio distributions for lab L6, plotting the value of $F_{1,n}(x) - F_{2,m}(x)$ (equation (3)) over the aspect ratio range of the data. The positive and negative values of the supremum are shown as dashed lines. The supremum is exceeded over two ranges of the aspect ratio, demonstrating that the cumulative distributions of Sample 1 and 2 are statistically different. The K–S two-sample test shows that all labs

reported aspect ratio distributions for the two samples that are statistically different from each other.

This non-parametric test establishes that the aspect ratio distributions of Samples 1 and 2 are different, but does not quantify the difference. The next section shows how the distributions can be modeled to give parameters that can be compared quantitatively.

3.4. Uncertainty of parameters fitted to reference models

3.4.1. Reference models fitted to size and shape descriptor cumulative distributions.—

Figures 7 and 8 show some output from the curve-fitting Shiny App® for Feret diameter and aspect ratio descriptors, respectively, for the Sample 2 data of lab L1. Figure 7(a) shows the Feret diameter density distributions while figure 7(b) shows the Feret diameter cumulative distributions. The data is represented as the black curve, the non-linear least squares regression fit is represented by the blue curve (NLS, blue), and the maximum likelihood fit is represented by the red curve (MLE). Figure 8(a) shows the aspect ratio density distributions, and figure 8(b) shows the aspect ratio cumulative distributions. Both the Feret and aspect ratio descriptor distributions appear to be multimodal for all reported datasets. For the data from lab L1, the normal distribution appeared to fit both the Feret and aspect ratio descriptor distributions. It is possible to deconvolute the descriptor distributions into subpeaks; however, the standard error of the fitted parameters would increase significantly, and much more data would be required to adequately resolve the peaks. Therefore, the nanorod distributions were fitted using unimodal reference models.

3.4.2. Uncertainty of fitted parameters.—

Table 3 compares uncertainties (U_{ILC}) of scale and width parameters for the size descriptors, Feret and minFeret. The grand averages of both the Feret and minFeret scale parameters are not statistically different from each other. However, the grand averages of the Feret and minFeret width parameters are statistically different between the two samples, e.g. the two averages are different by more than two standard deviations of their values. Of the two size descriptors, the Feret diameter might be preferred because it has smaller uncertainties than those of the minFeret diameter. However, within each laboratory, the coefficients of variation for scale parameters are less than 0.1%, and the coefficients of variation for width parameters are less than 0.5%. All labs reported significant differences between the width parameters for the Feret and minFeret descriptors of both samples.

3.4.3. Elongational shape descriptor: the aspect ratio.—

As shown in table 3, the grand average aspect ratio scales for Samples 1 and 2 are within two standard deviations of each other, and are statistically similar. However, the grand average aspect ratio widths are distinctly different. The differences between the widths of these distributions show that the two samples are statistically different. This information could be used to distinguish between the two samples, which, in turn, could be used to modify synthesis processes to accentuate or reduce the difference. This information could also be used to address regulatory issues.

4. Discussion

This section provides additional evaluations of descriptor interlaboratory reproducibility, identifies univariate and bivariate descriptor visualizations that aid analysis, and provides estimates of LSPR based on nanorod dimensions.

4.1. Interlaboratory reproducibility of nanorod descriptors

Table 3 shows the coefficients of variation and uncertainties for the scale and width parameters of three nanorod descriptors: the Feret diameter, minFeret diameter, and aspect ratio. Here, we provide a summary of causes for the uncertainty values; additional material and discussion of causes for interlaboratory reproducibility are provided in section 5 of the SI. Gold nanorods undergo capillary flow-driven self-assembly when deposited on TEM grids (Sharma et al 2009a). The transitions between smectic and nematic morphologies depend on the areal density of the sample on the grid and the average aspect ratio of the nanorods (see table SI-1). The potential effects of the calibration method, pixel resolution, number of particles analyzed, and number of images analyzed were evaluated using ANOVA methods; however, none of these factors appear to describe differences between the interlaboratory reproducibility of descriptor datasets. Raw data triage resulted in removal of 1–5% of the measured nanorods in various laboratories. A comparison of interlaboratory reproducibility between this study and one for gold nanospheres is shown in table 4. The grand means of scale and width parameters for the equivalent circular diameter of a gold nanosphere reference material are shown in the third row of this table. RM8012 is certified for its equivalent circular diameter, a scale parameter that has a measurement uncertainty of 5.74%, but not its width parameter, which has a measurement uncertainty of 31.4%. The two nanorod samples of this study (Sample 1 = S1; Sample 2 = S2) have higher measurement uncertainties of their scale parameters (16.9% and 13.5%, respectively), but not their width parameters (16.3% and 12.0%, respectively). Interestingly, the measurement uncertainties of the scale and width parameters of the aspect ratio descriptors are about 5% and 3%, respectively, for both Sample 1 and Sample 2. We are able to discriminate between these two samples by using their aspect ratio data, which has the lowest measurement uncertainties for any of the descriptors reported. Table 4 also reports the relative spread of the length and aspect ratio distributions between the two studies. Sample 2 has smaller relative spreads of each descriptor than Sample 1, which is additional evidence that the samples are different.

4.2. Distribution visualizations

4.2.1. Univariable distributions.—Quantile plots can be used to illustrate the quality of the model fit for a distribution over the full range of descriptor data. Figures 9 and 10 are quantile plots comparing the Sample 1 and 2 distributions for the Feret diameters and aspect ratios reported by lab L1. The X-axis shows the values for the descriptor, and the Y-axis transforms the cumulative distribution data into quantiles using the normal distribution model. Each integer value of Y corresponds to a standard deviation from the mean. The mean values of the Feret diameters of Sample 1 and 2 were 58.6 nm and 57.9 nm, respectively. However, the widths of these distributions were different, e.g. 7.62 nm for Sample 1 and 5.49 nm for Sample 2. The normal models for both samples fit the data well over the range $-2 < Y < 2$, or ±2 standard deviations. As shown in figure 9, the slope of the

Sample 2 distribution is steeper because standard deviation was smaller than that of Sample 1. The mean values of the aspect ratio scale parameters of Samples 1 and 2 were 0.362 and 0.343, respectively (figure 10). The widths of the aspect ratio width parameters of Samples 1 and 2 were distinctly different, with values of 0.0611 and 0.0391, respectively.

Hubert and coworkers (2010) analyzed a bifurcation mechanism for seed-mediated syntheses of gold nanorods. For this particular recipe, the growth processes of nanorods and nanocubes appeared to differentiate above a critical size of 5 nm. The ratios of the length-to-width growth rates were determined by the slope of the nanorod line on a plot of the minFeret diameter versus the Feret diameter. In addition to relating to the bifurcation growth mechanism, this bivariate plot provides another method for visualizing the distribution of nanorod aspect ratios. Their method uses a coordinate transformation based on the centroid and nanorod line of this plot, generating two independent, normal distributions for the axial and transverse directions. This approach links the growth rate mechanisms to the final size distribution of the product. Figure 11 shows a plot for the Sample 1 data of lab L6. The nanocubes are shown as open red squares. The red line shows an aspect ratio of one, corresponding to a perfect nanocube or nanosphere. The nanorods are shown as black open bars. The fitted black line represents an average location of the nanorods in the Feret–minFeret plane. The intersection of the red and black lines is considered the bifurcation point (Hubert et al 2010), which is (13.7 nm, 13.7 nm) for Sample 1.

For this analysis of the lab L6 dataset (Hubert et al 2010), the widths of the axial and transverse distributions for Sample 1 are statistically larger than those of Sample 2. Each laboratory dataset in this study showed analogous results. Similar quantitative trends are shown in the Feret and minFeret width distribution data shown in table 3. However, the uncertainties of the Hubert analysis parameters are higher, possibly due to the uncertainty associated with low R^2 values associated with the nanorod line coefficients. Bivariate Feret–minFeret histograms provide another way of visualizing the differences in aspect ratios between Samples 1 and 2. Figure 12 shows such histograms for Samples 1 and 2 of the lab L6 datasets. The Sample 1 dataset has a broader base and is less than one-half the height of the Sample 2 dataset.

4.3. Prediction of LSPR using distribution data

Predictions of shape (or size)-based physical properties could be an outcome of measuring and modeling size and shape distributions of nanorods. An incentive for generating size and shape distributions for nanorod dispersions is to predict their anisotropic properties. Brioude et al (2005) developed a linear correlation between the longitudinal resonance maximum for gold nanorods as a function of their aspect ratios. The prediction is based on classical electrostatic predictions, the absorption cross-sections of the particles, and the assumption that gold nanorods behave as ellipsoidal particles. The equation was as follows:

$$\lambda_{\max} = 96\ \text{nm} \cdot \text{shape factor} + 418\ \text{nm} \tag{7}$$

where λ_{max} is the maximum in the longitudinal resonance, and the shape factor is the inverse of the aspect ratio. An alternative approach was proposed by Juve et al (2013). Their study showed that the measured LSPR broadened with reductions in both nanorod diameter

and nanorod length, which is thought to be linked to a surface broadening contribution. They proposed using an effective confinement length (ECL) to model this effect:

$$\mathrm{ECL} = \sqrt{W \cdot L} \tag{8}$$

where W and L are the minFeret and Feret diameters, respectively.

Of course, nanorod size and shape distributions measured by TEM can be used to estimate the key variable in either model for any sample. Figure 13 shows the plot of the ECL as a function of nanorod aspect ratio for the data of lab L6. Bivariate analysis of these plots shows that the distributions are not similar ($p < 0.001$), confirming that the ECL distribution would be different for the two samples. As demonstrated in this contour plot, Sample 1 has a broader distribution in both the Feret and minFeret ranges, and the maximum distribution height is about half that of Sample 2.

5. Conclusions

The key objective was to determine whether two different samples, which had different performance attributes in their application, were different with respect to their descriptor distributions. The raw triage workflow included the following: identifying whether non-nanorod particles were present, developing descriptor criteria for detecting touching particles in images, developing descriptor criteria for differentiation between nanorods and nanocubes, and identifying size and shape descriptors with high repeatability (intralaboratory) and reproducibility (interlaboratory). Some as-received datasets reported touching particles and non-rod shapes that were not to be evaluated. The solidity descriptor, a ruggedness shape factor, was particularly applicable to identifying touching particles, for which the area of the agglomerate convex hull is usually much larger than the measured agglomerate area. In these nanorod samples, discrete nanoparticles had solidities greater than 0.90. This condition was used to automate the sorting and removal process for touching particles. Similarly, the aspect ratio descriptor had a narrow range of values for non-nanorod (nanocube) particles and was used to automate the process of removing nanocubes. Figure SI-5 of SI illustrates the decision tree for the automation of selecting nanorod particles from complex images. Samples were differentiated by computing the K-S statistic for their empirical cumulative distributions. Reference model parameters were fitted to size and shape descriptor distributions. Uncertainties were estimated for the fitted parameters from three descriptor distributions: the Feret diameter, minimum Feret diameter, and aspect ratio. The normal distribution provided the best overall fit to the Feret diameter and aspect ratio descriptors. The Feret diameter is the preferred size descriptor since the uncertainties of its scale and width parameters were generally better that those of the minimum Feret diameter. The two samples were differentiated using the width parameter values of the Feret diameter, minFeret diameter, or aspect ratio distributions. Sample 1 had larger width parameter values, i.e. these distributions were broader than those of Sample 2. Visualizations of the distributions over their descriptor ranges helped confirm the findings. Quantitative size and shape distributions might be used to estimate LSPR results or the performance of separation technologies. For example, the nanorod length scale histograms showed that the sample with smaller width parameters had a much narrower bivariate distribution. Estimates of the LSPR

distribution suggest that this sample would have a more confined response. These methods can be fully automated, which could make critical analysis of nanoparticle size and shape distributions a practical reality.

Supplementary Material

Refer to Web version on PubMed Central for supplementary material.

Acknowledgments

The authors thank Toshiyuki Fujimoto and Naoyuki Taketoshi of AIST for their advice and counsel with respect to ISO/TC229 needs and requirements of this study. The authors also thank the following researchers at National Institute of Standards and Technology (NIST) for their useful critiques regarding this study: Angela Hight Walker and Jeff Fagan. The work by AIST was part of the research program of ‘strategic international standardization acceleration projects’ supported by the Ministry of Economy, Trade, and Industry of Japan. The work by KRISS was part of the Nano Material Technology Development Program (2014M3A7B6020163) of Ministry of Science, ICT, and Future Planning/National Research Foundation (MSIP/NRF). The findings and conclusions in this report are those of the authors and do not necessarily represent the views of the US National Institute for Occupational Safety and Health.

References

Alkilany AM, Thompson LB, Boulos SP, Sisco PN and Murphy CJ 2012 Gold nanorods: their potential for photothermal therapeutics and drug delivery, tempered by the complexity of their biological interactions Adv. Drug Deliv. Rev 64 190–9 [PubMed: 21397647]

Bau S, Witschger O, Gensdarmes F, Rastoix O and Thomas D 2010 A TEM-based method as an alternative to the BET method for measuring off-line the specific surface area of nanoaerosols Powder Technol. 200 190–201

Becker J, Trugler A, Jacab A, Hohenester U and Sonnischsen C 2010 The optimal aspect ratio of gold nanorods for plasmonic bio-sensing Plasmonics 5 161–7

Bell NC, Minelli C, Tompkins J, Stevens MM and Shard AG 2012 Emerging techniques for submicrometer particle sizing applied to Stober silica Langmuir 28 10860–72 [PubMed: 22724385]

Bolhuis P and Frenkel D 1997 Tracing the phase boundaries of hard spherocylinders J. Chem. Phys 106 666–87

Braun A, Couteau O, Franks K, Kestens V, Roebben G, Lamberty A and Linsinger TPJ 2011 Validation of dynamic light scattering and centrifugal liquid sedimentation methods for nanoparticle characterisation Adv. Powder Technol 22 766–70

Brioude A, Jiang XC and Pileni MP 2005 Optical properties of gold nanorods: DDA simulations supported by experiments J. Phys. Chem. B 109 13138–42 [PubMed: 16852635]

Chen S, Huang H, Zhang L, Chen Y and Liu X 2016 Alternate release of different target species based on the same gold nanorods and monitored by cell imaging Colloids Surf. B 145 671–8

De Temmerman P-J, Lammertyn J, De Ketelaere B, Kestens V, Roebben G, Verleysen E and Mast J 2014 Measurement uncertainties of size, shape, and surface measurements using transmission electron microscopy of nearmonodisperse, near-spherical nanoparticles J. Nanopart. Res 16 2177

Dembereldorj U, Choi SY, Ganbold E-O, Song NW, Kim D, Choo J, Lee SY, Kim S and Joo S-W 2014 Gold nanorod-assembled PEGylated graphene-oxide nanocomposites for photothermal cancer therapy Photochem. Photobiol 90 659–66 [PubMed: 24303894]

Du L, Furube A, Yamamoto K, Hara K, Katoh R and Tachiya M 2009 Plasmon-induced charge separation and recombination dynamics in gold-TiO_2 nanoparticle systems: dependence on TiO_2 particle size J. Phys. Chem. C 113 6454–62

Grulke EA et al. 2018 Size and shape distributions of carbon black aggregates by transmission electron microscopy Carbon 130 822–33

Grulke EA et al. 2017 Size and shape distributions of primary crystallites in titania aggregates Adv. Powder Technol 28 1647–59 [PubMed: 29200658]

GSB 2013 National certified reference material 02-2994-2013 (People's Repubic of China) p 5

Henkel A, Schubert O, Plech A and Soennichsen C 2009 Growth kinetic of a rod-shaped metal nanocrystal J. Phys. Chem. C 113 10390–4

Hentschel ML and Page NW 2003 Selection of descriptors for particle shape characterization Part. Part. Syst. Charact 20 25–38

Hu Z, Ji Y, Hou S and Wu X 2014a Minimizing the effect of near-distance dielectric sensitivity on retrieving average aspect ratio of gold nanorod by optical extinction spectroscopy in the case of CTAB adsorption Chin. Sci. Bull 59 1822–31

Hu ZJ, Hou S, Ji YL, Wen T, Liu WQ, Zhang H, Shi XW, Yan J and Wu XC 2014b Fast characterization of gold nanorods ensemble by correlating its structure with optical extinction spectral features AIP Adv. 4 117137

Huang X, Jain PK, El-Sayed IH and El-Sayed MA 2007 Gold nanoparticles: interesting optical properties and recent applications in cancer diagnostics and therapy Nanomedicine 2 681–93 [PubMed: 17976030]

Huang X, Neretina S and El-Sayed MA 2009 Gold Nanorods: from synthesis and properties to biological and biomedical applications Adv. Mater 21 4880–910 [PubMed: 25378252]

Hubert F, Testard F, Rizza G and Spalla O 2010 Nanorods versus nanospheres: a bifurcation mechanism revealed by principal component TEM analysis Langmuir 26 6887–91 [PubMed: 20405865]

Hubert F, Testard F, Thill A, Kong Q, Tache O and Spalla O 2012 Growth and overgrowth of concentrated gold nanorods: time resolved SAXS and XANES Cryst. Growth Des 12 1548–55

ISO 9276-6 2008 Representation of Results of Particle Size Analysis—Part 6: Descriptive and Quantitative Representation of Particle Shape and Morphology (Geneva: ISO) p 23

Jana NR, Gearheart L, Obare SO and Murphy CJ 2002 Anisotropic chemical reactivity of gold spheroids and nanorods Langmuir 18 922–7

JCBM/WG1 2008 Evaluation of Measurement Data—Guide to the Expression of Uncertainty in Measurement (Paris: Bureau International des Poids et Mesures) (JCGM 100:2008)

Juve V, Cardinal MF, Lombardi A, Crut A, Maioli P, Perez-Juste J, Liz-Marzan LM, Del Fatti N and Vallee F 2013 Size-dependent surface plasmon resonance broadening in nonspherical nanoparticles: single gold nanorods Nano Lett. 13 2234–40 [PubMed: 23611370]

Kestens V and Roebben G 2014 Certification Report—the Certification of Equivalent Diameters of a Mixture of Silica Nanoparticles in Aqueous Solution: ERM-FD102 (Geel: IRMM)

Khlebtsov BN, Khanadeev VA and Khlebtsov NG 2014 Extinction and extra-high depolarized light scattering spectra of gold nanorods with improved purity and dimension tunability: direct and inverse problems Phys. Chem. Chem. Phys 16 5710–22 [PubMed: 24522336]

Klein T, Buhr E, Johnsen KP and Frase CG 2011 Traceable measurement of nanoparticle size using a scanning electron microscope in transmission mode (TSEM) Meas. Sci. Technol 22 094002

Kou SF, Ye W, Guo X, Xu XF, Sun HY and Yang J 2016 Gold nanorods coated by oxygen-deficient TiO_2 as an advanced photocatalyst for hydrogen evolution RSC Adv. 6 39144–9

Linsinger T, Roebben G, Gilligand D, Calzolai L, Rossi F, Gibson N and Klein C 2012 Requirements of Measurements for the Implementation of the European Commission Definition of the Term 'Nanomaterial' ed European Commission (Geel, Belgium: Joint Research Centre of the European Commission, Institute for Reference Materials and Measurements) (10.2787/63490)

Masuda H and Gotoh K 1999 Study on the sample size required for the estimation of mean particle diameter Adv. Powder Technol 10 159–73

Masuda H and Iinoya K 1970 Theoretical study of the scatter of experimental data due to particle-size-distribution J. Chem. Eng. Japan 4 60–6

Mohamed MB, Volkov V, Link S and El-Sayed MA 2000 The 'lightning' gold nanorods: fluorescence enhancement of over a million compared to the gold metal Chem. Phys. Lett 317517–23

Morita T, Hatakeyama Y, Nishikawa K, Tanaka E, Shingai R, Murai H, Nakano H and Hino K 2009 Multiple small-angle x-ray scattering analyses of the structure of gold nanorods with unique end caps Chem. Phys 364 14–8

Murphy CJ, Gole AM, Stone JW, Sisco PN, Alkilany AM, Goldsmith EC and Baxter SC 2008 Gold nanoparticles in biology: beyond toxicity to cellular imaging Acc. Chem. Res 41 1721–30 [PubMed: 18712884]

Murphy CJ, Sau TK, Gole AM, Orendorff CJ, Gao J, Gou L, Hunyadi SE and Li T 2005 Anisotropic metal nanoparticles: synthesis, assembly, and optical applications J. Phys. Chem. B 109 13857–70 [PubMed: 16852739]

Nguyen TM, Liu J and Hackley VA 2015 Fractionation and characterization of high aspect ratio gold nanorods using asymmetric-flow field flow fractionation and single particle inductively coupled plasma mass spectrometry Chromatography 2 422–35

Nguyen TM, Pettibone JM, Gigault J and Hackley VA 2016 *In situ* monitoring, separation, and characterization of gold nanorod transformation during seed-mediated synthesis Anal. Bioanal. Chem 408 2195–201 [PubMed: 26873210]

Nikoobakht B, Wang J and El-Sayed MA 2002 Surface-enhanced Raman scattering of molecules adsorbed on gold nanorods: off-surface plasmon resonance condition Chem. Phys. Lett 366 17–23

Nontapot K, Rastogi V, Fagan JA and Reipa V 2013 Size and density measurement of core-shell Si nanoparticles by analytical ultracentrifugation Nanotechnology 24 155701 [PubMed: 23518716]

Perez-Juste J, Pastoriza-Santos I, Liz-Marzan LM and Mulvaney P 2005 Gold nanorods: synthesis, characterization and applications Coord. Chem. Rev 249 1870–901

Prescott SW and Mulvaney P 2006 Gold nanorod extinction spectra J. Appl. Phys 99 123504

Rice SB et al. 2013 Particle size distributions by transmission electron microscopy: an interlaboratory comparison case study Metrologia 50 663–78 [PubMed: 26361398]

Rizzo ML and Szekely GJ 2016 Energy distance Wiley Interdiscip. Rev. Comput. Stat 8 27–38

Schindelin J, Rueden CT, Hiner MC and Eliceiri KW 2015 The ImageJ ecosystem: an open platform for biomedical image analysis Mol. Reprod. Dev 82 518–29 [PubMed: 26153368]

Schmucker AL, Harris N, Banholzer MJ, Blaber MG, Osberg KD, Schatz GC and Mirkin CA 2010 Correlating nanorod structure with experimentally measured and theoretically predicted surface plasmon resonance ACS Nano 4 5453–63 [PubMed: 20738131]

Sharma V, Park K and Srinivasarao M 2009a Colloidal dispersion of gold nanorods: historical background, optical properties, seed-mediated synthesis, shape separation and self-assembly Mater. Sci. Eng. R R65 1–38

Sharma V, Park K and Srinivasarao M 2009b Shape separation of gold nanorods using centrifugation Proc. Natl Acad. Sci. USA 106 4981–5 [PubMed: 19255445]

Song NW, Park KM, Lee I-H and Huh H 2009 Uncertainty estimation of nanoparticle size distribution from a finite number of data obtained by microscopic analysis Metrologia 46 480–8

Souza DOC and Menegalli FC 2011 Image analysis: statistical study of particle size distribution and shape characterization Powder Technol. 214 57–63

Szekely GJ and Rizzo ML 2004 Testing for Equal Distributions in High Dimension (Bowling: Green State University)

Takahashi K, Kato H, Saito T, Matsuyama S and Kinugasa S 2008 Precise measurement of the size of nanoparticles by dynamic light scattering with uncertainty analysis Part. Part. Syst. Charact 25 31–8

Wang LC et al. 2011 Selective targeting of gold nanorods at the mitochondria of cancer cells: implications for cancer therapy Nano Lett. 11 772–80 [PubMed: 21186824]

Zhang Z, Wang J, Nie X, Wen T, Ji Y, Wu X, Zhao Y and Chen C 2014 Near infrared laser-induced targeted cancer therapy using thermoresponsive polymer encapsulated gold nanorods J. Am. Chem. Soc 136 7317–26 [PubMed: 24773323]

Zhang Z, Wang L, Wang J, Jiang X, Li X, Hu Z, Ji Y, Wu X and Chen C 2012 Mesoporous silica-coated gold nanorods as a light-mediated multifunctional theranostic platform for cancer treatment Adv. Mater 24 1418–23 [PubMed: 22318874]

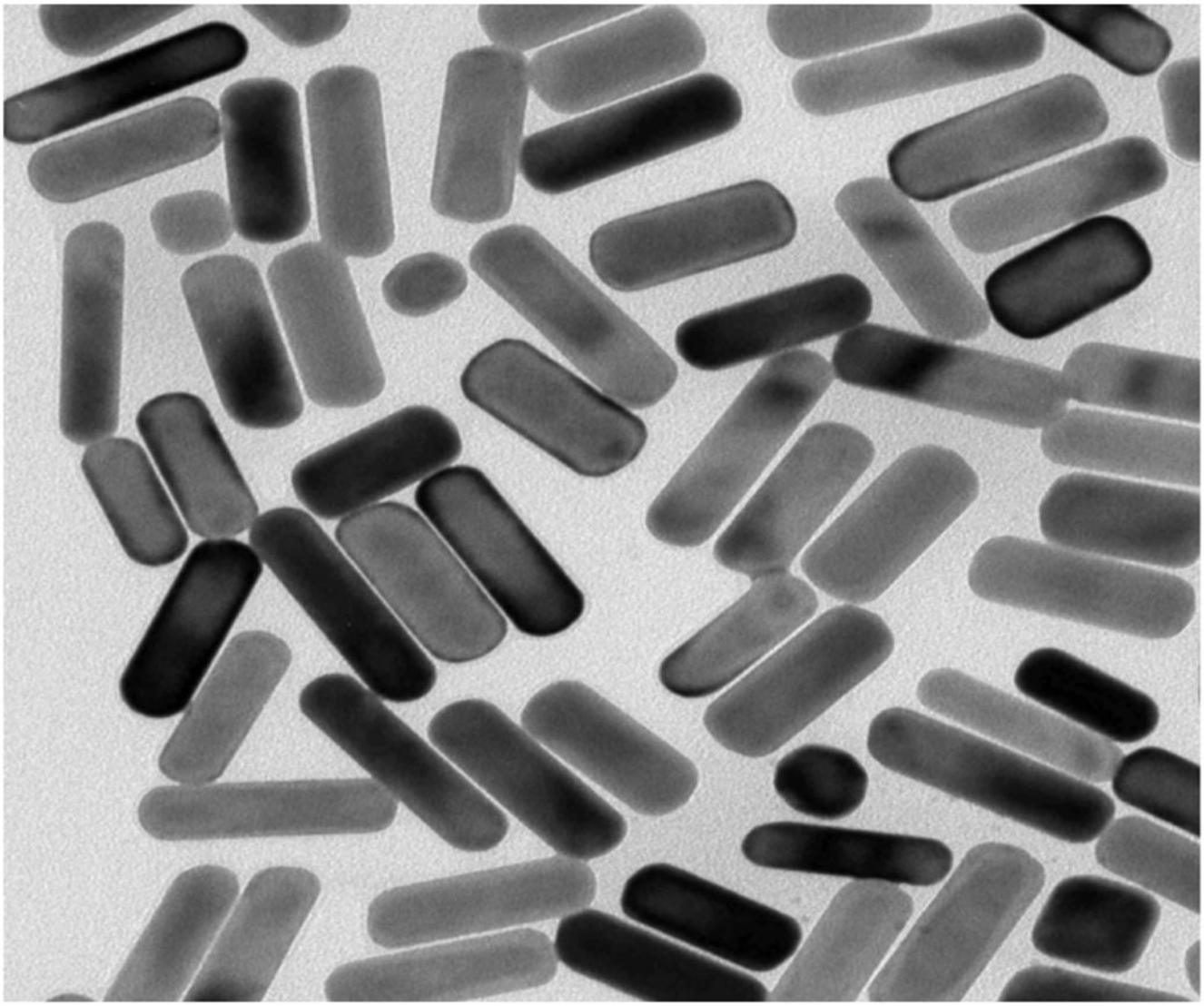

Figure 1.
TEM image of colloidal gold nanorods. Courtesy of AIST; MAG*I*CAL calibration, 0.1543 nm/pixel, Carl Zeiss EM-922, 200 kV. X 63k magnification.

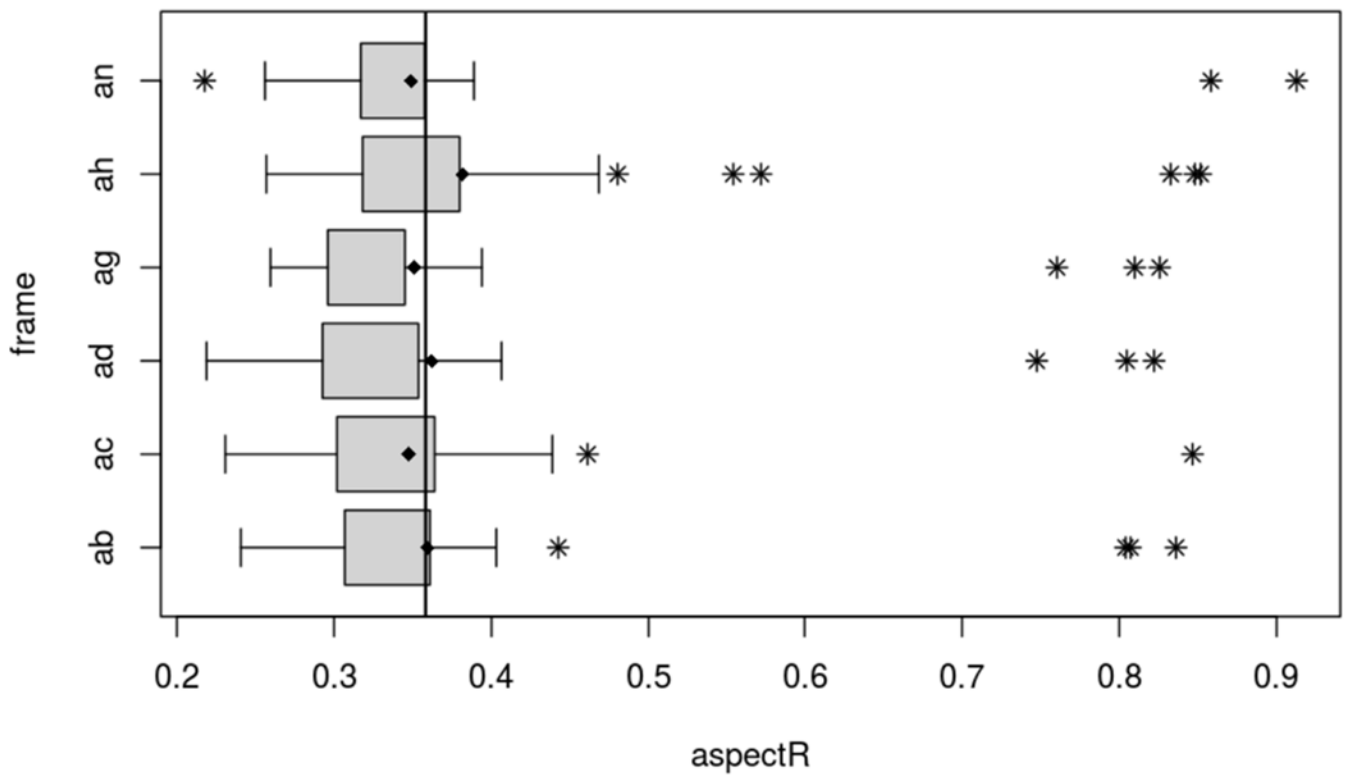

Figure 2.
Intralaboratory ANOVA (lab L2) of aspect ratio, six TEM images (images), Sample 2. Black vertical line = grand mean of aspect ratio descriptor; black diamonds = image means, gray box = ±1.5 standard deviation from the image mean, and extreme points (*) are greater than several standard deviations from the image mean.

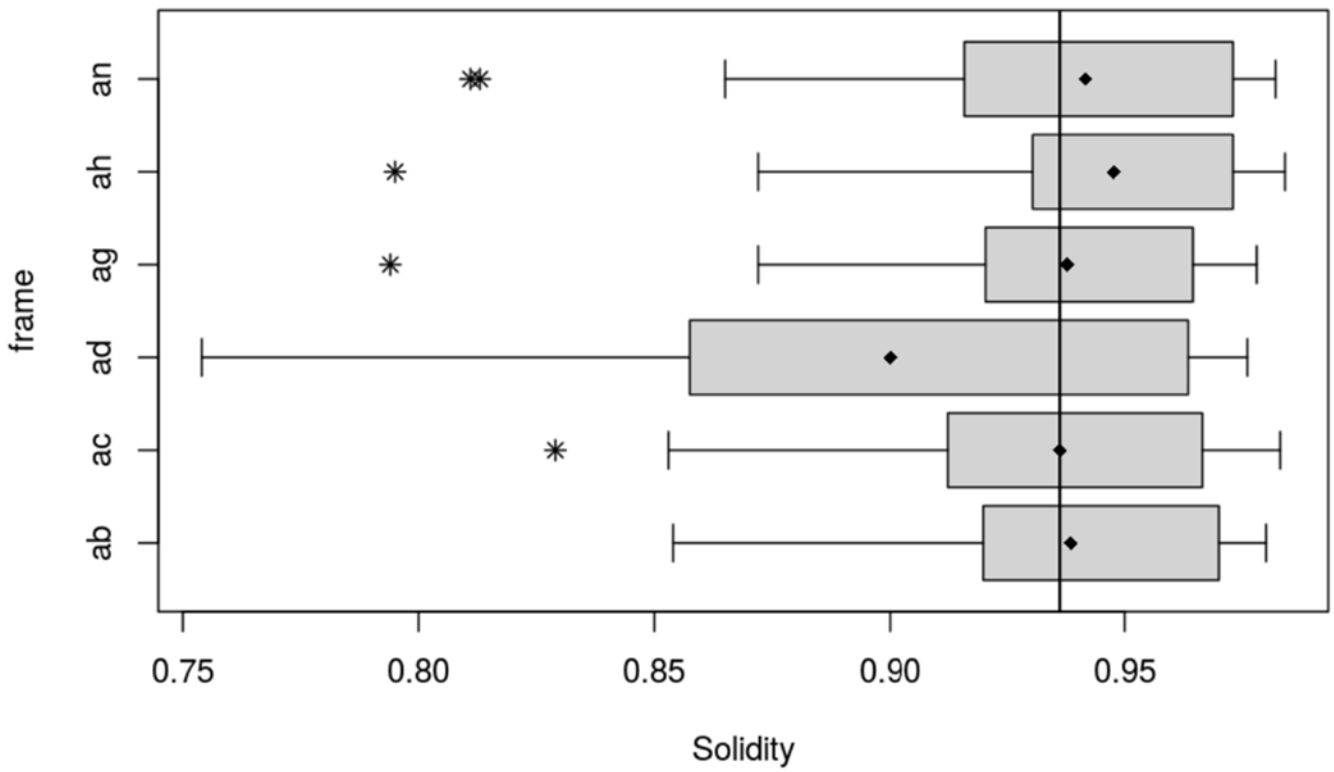

Figure 3.
ANOVA analysis of solidity data, Sample 2, lab L2, six TEM images. Black vertical line = grand mean of all images; black diamonds = image means, gray box = ±1.5 standard deviations from the image mean, and extreme points (*) are greater than several standard deviations from the image mean.

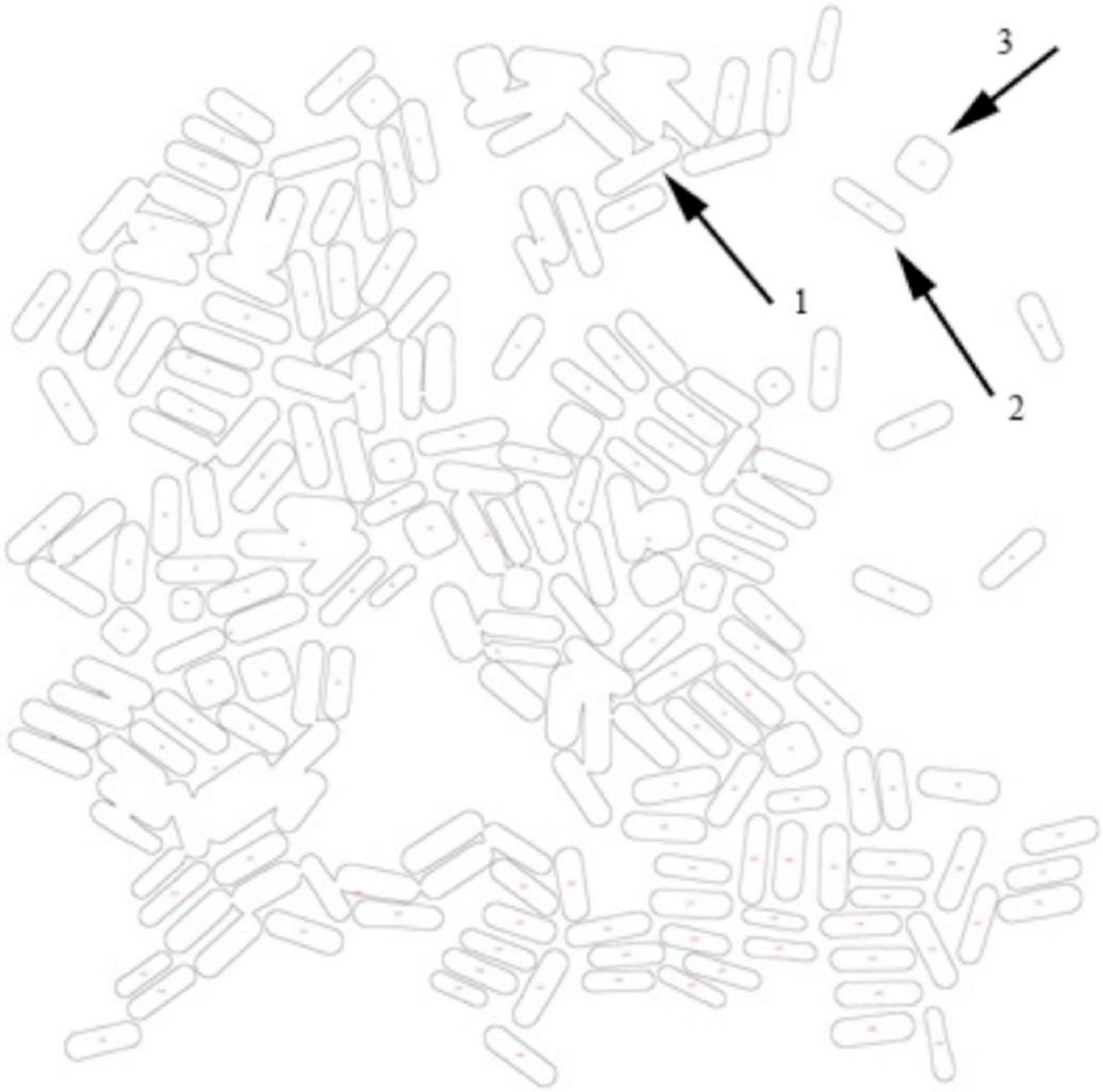

Figure 4.
ImageJ outline drawing of gold nanoparticles on a TEM support. Arrow 1 = touching particles; Arrow 2 = discrete nanorod; Arrow 3 = discrete nanocube.

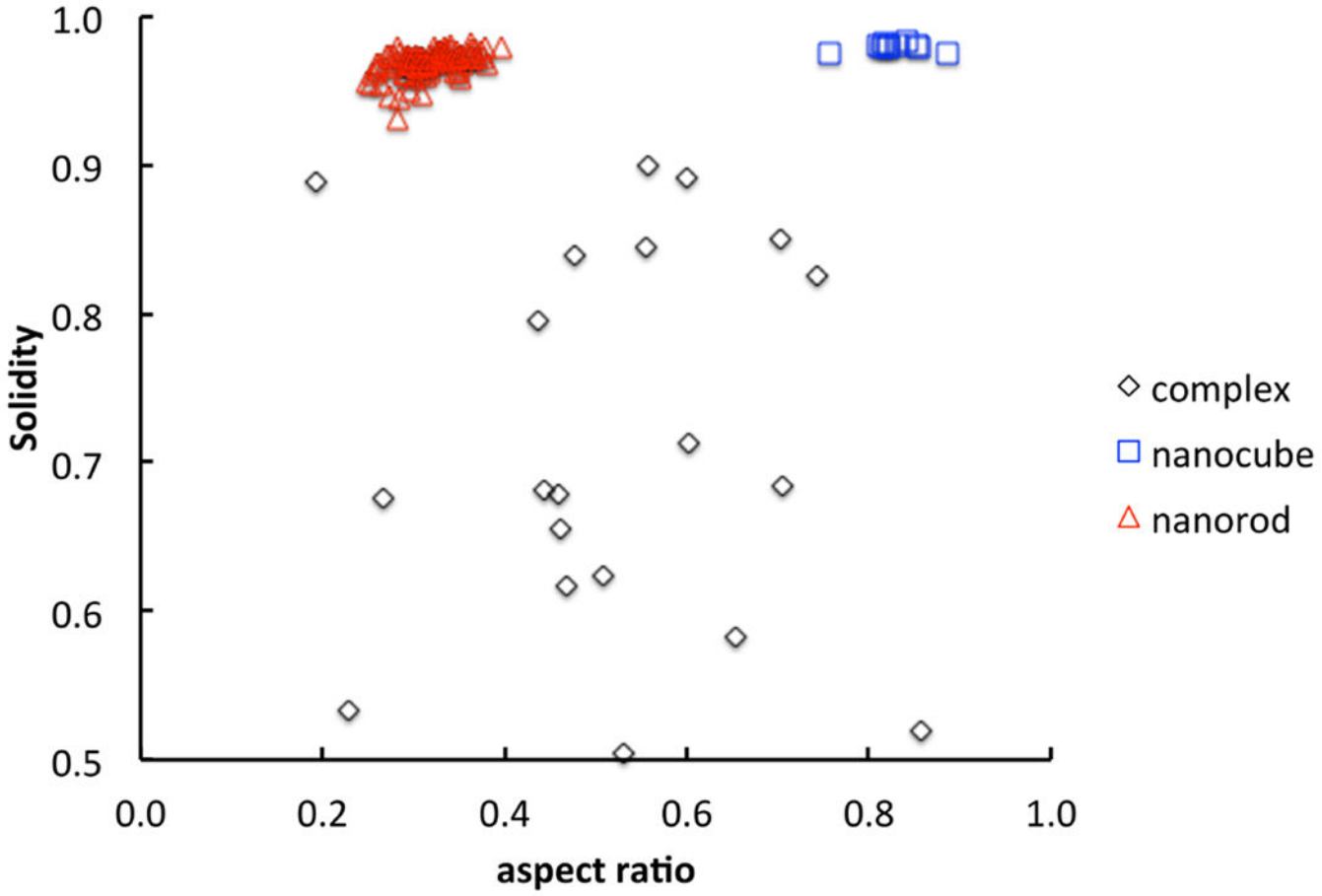

Figure 5.
Solidity versus aspect ratio for touching particles, nanocubes, and nanorods (arrows 1, 2, and 3, respectively of figure 4).

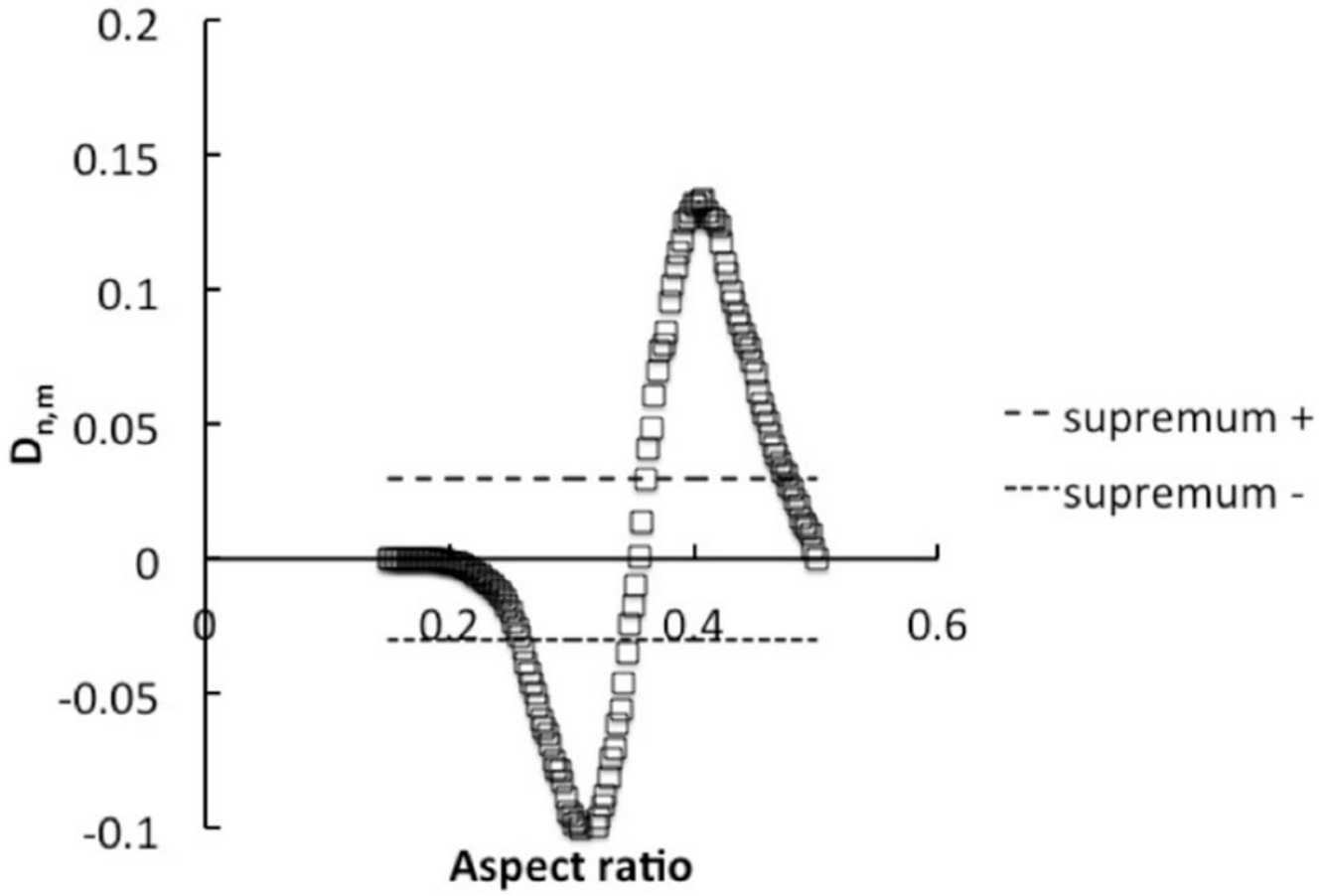

Figure 6.
Empirical cumulative distribution differences, lab L6.

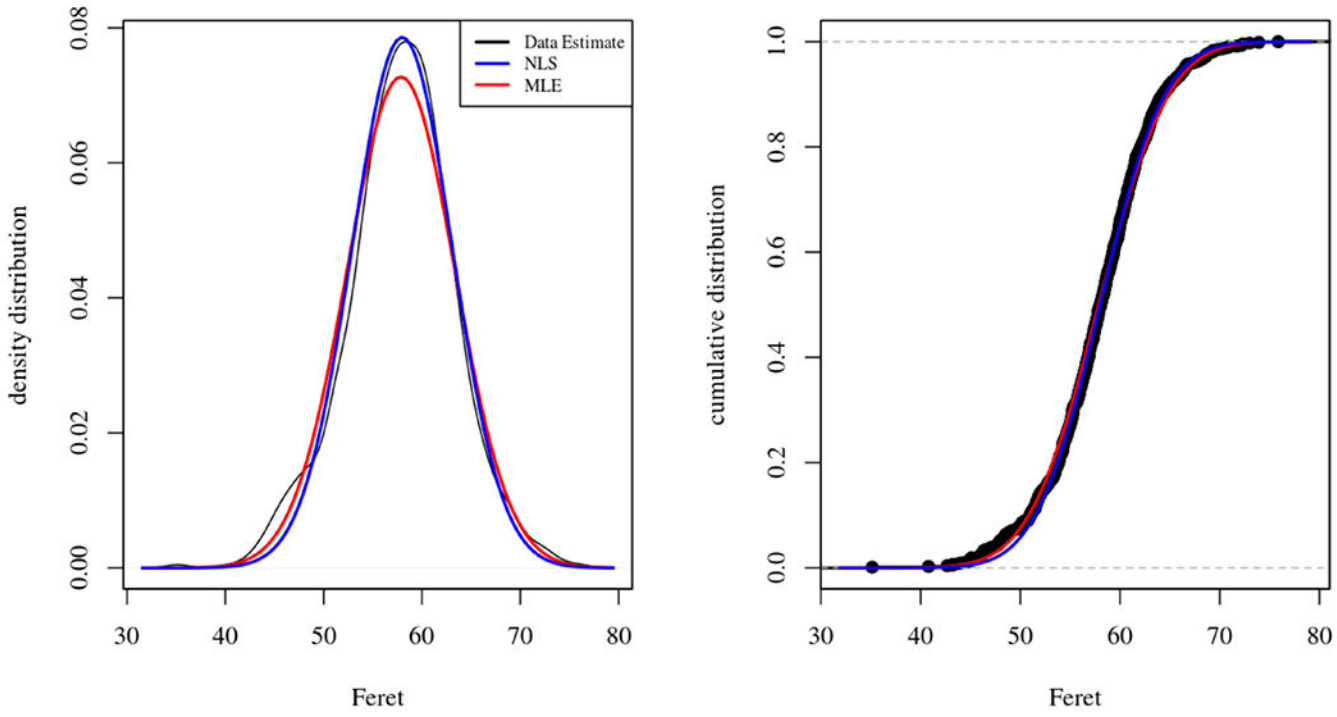

Figure 7.

Density and cumulative distributions, Feret diameter (nm), Sample 2, lab L1. Black line = smoothed data, black circles = cumulative distribution data, blue line = non-linear regression of fitted normal distribution, red line = maximum likelihood estimate of fitted normal distribution.

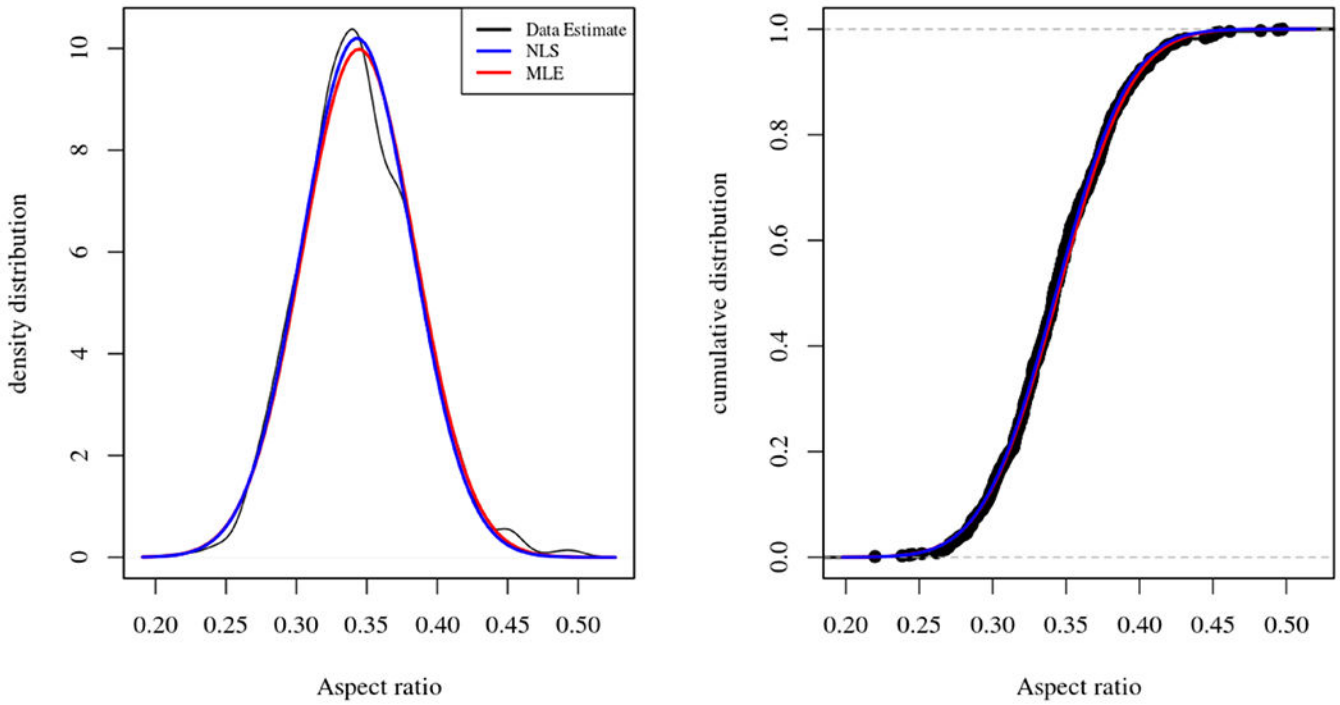

Figure 8.

Density and cumulative distributions, aspect ratio, Sample 2, lab L1. Black line = smoothed data, black circles = cumulative distribution data, blue line = non-linear regression of fitted normal distribution, red line = maximum likelihood estimate of fitted normal distribution.

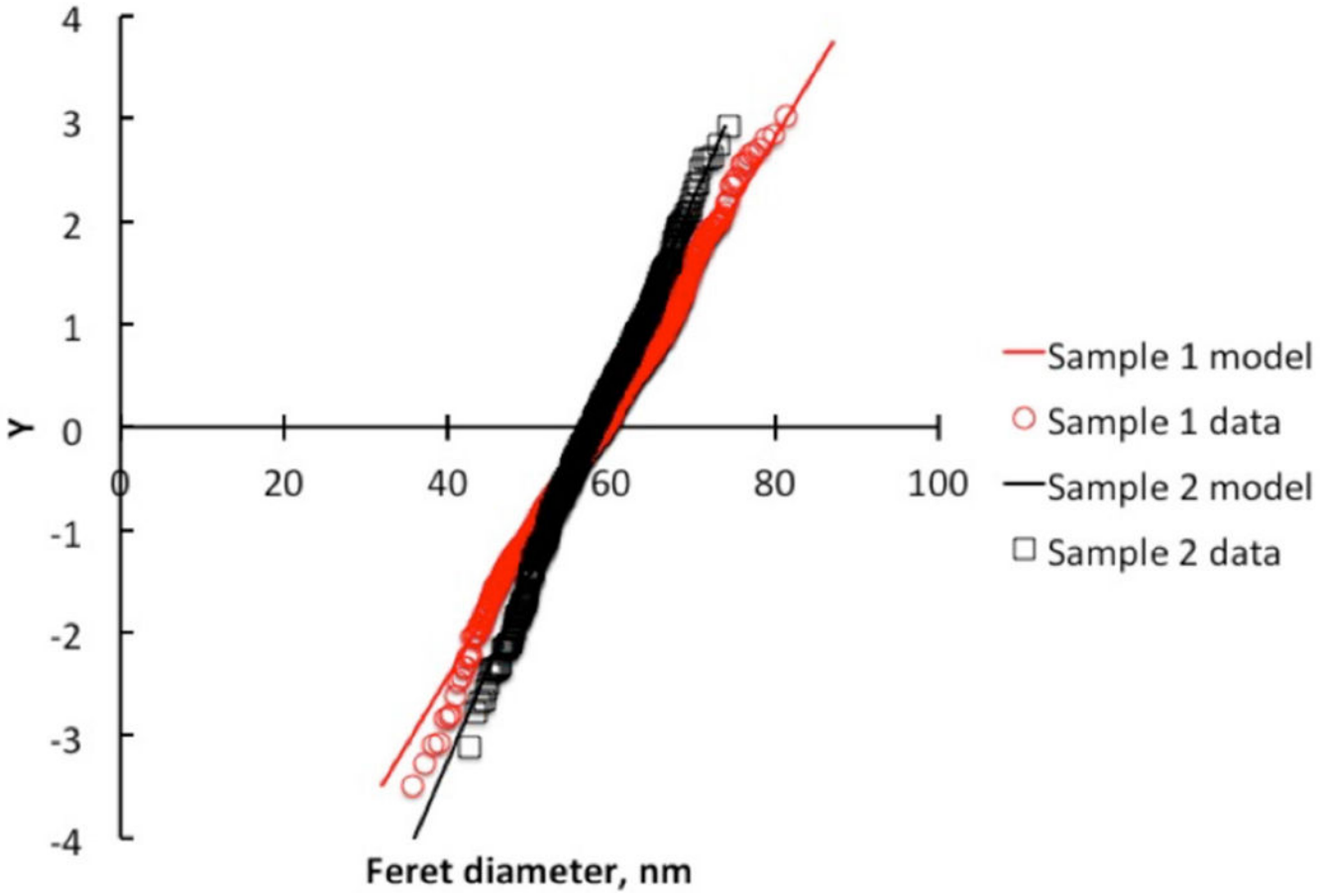

Figure 9.
Quantile plot of Feret diameter and its model, Samples 1 and 2, lab L1.

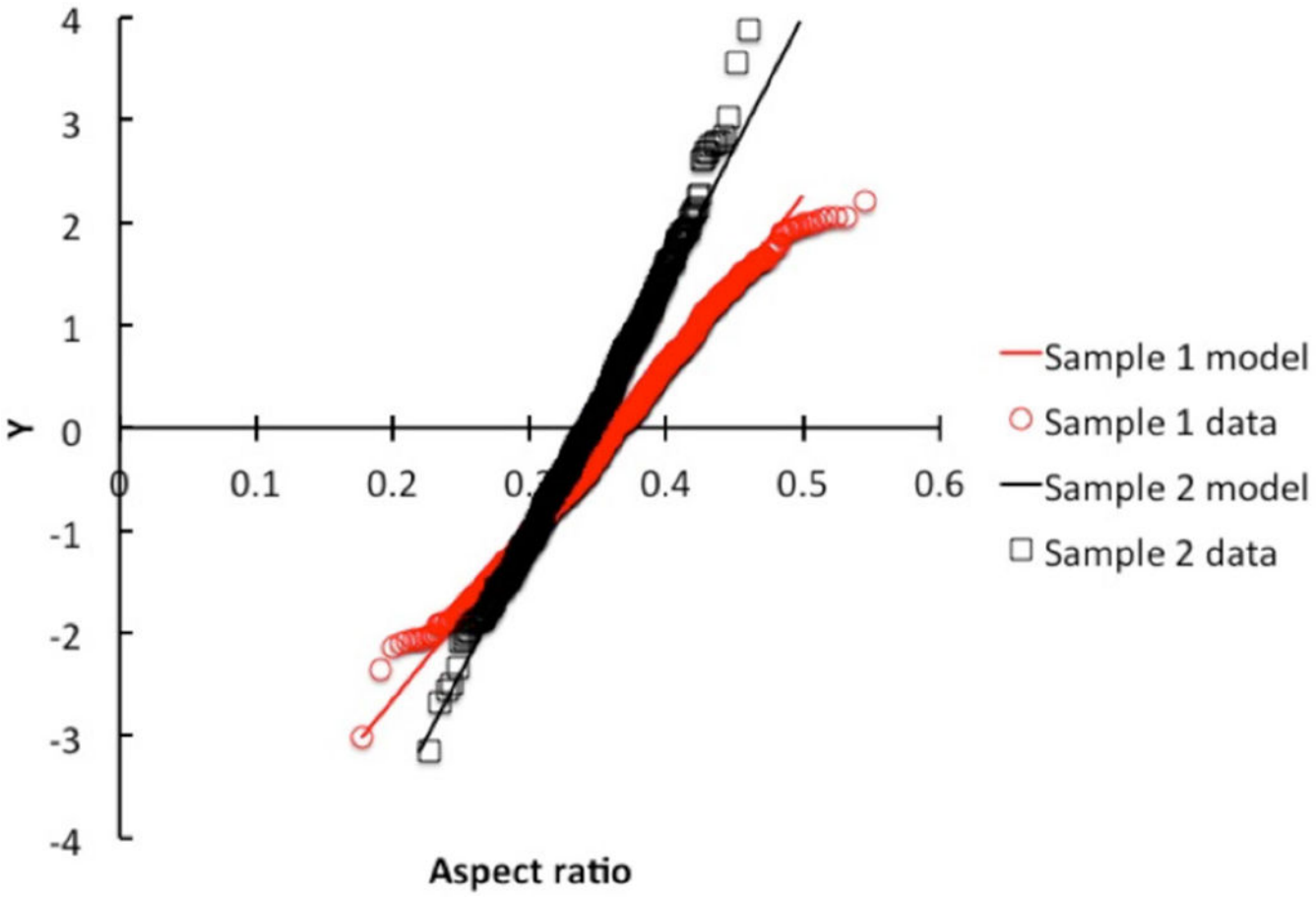

Figure 10.
Quantile plot of aspect ratio, Samples 1 and 2, lab L1.

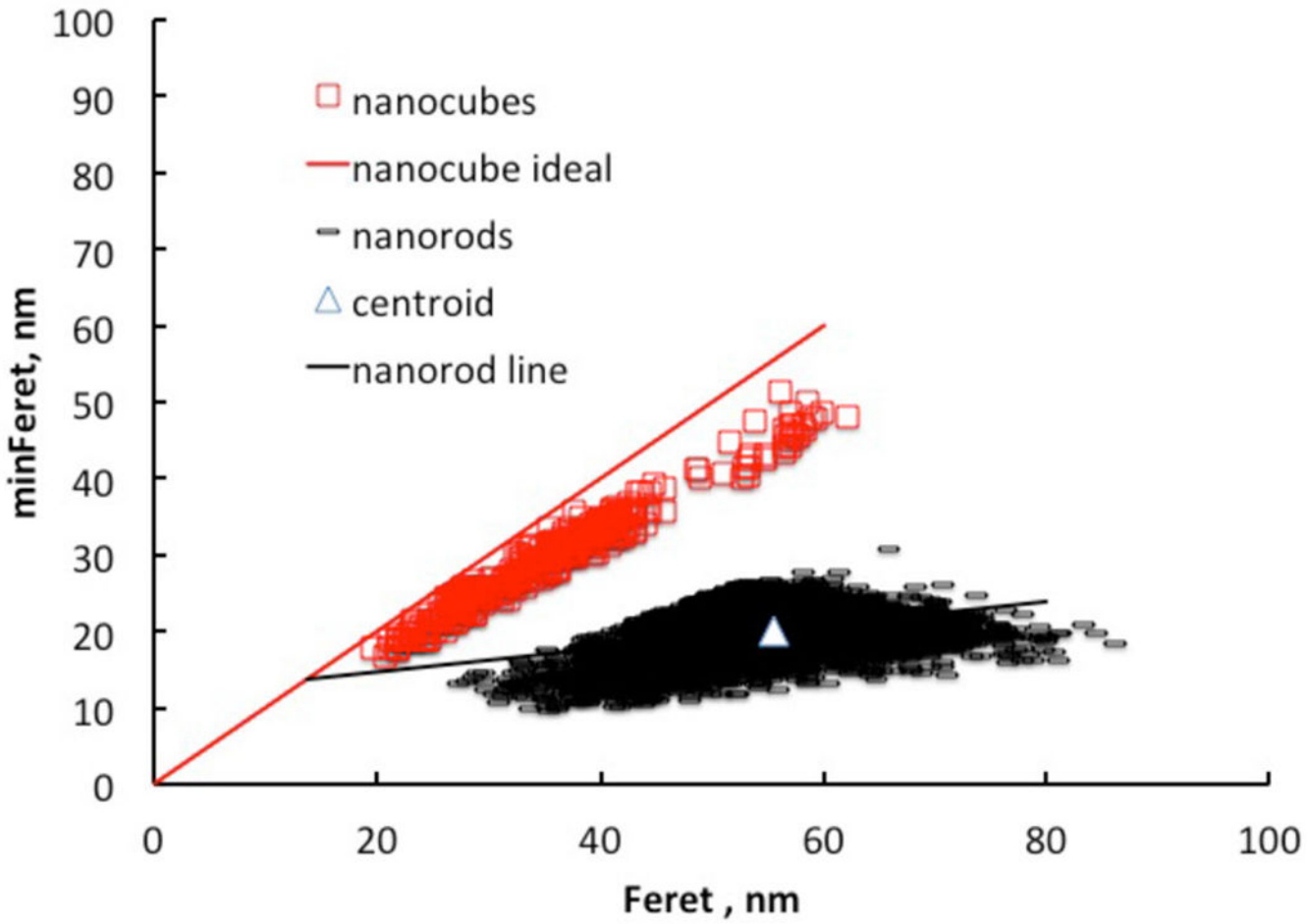

Figure 11.
Nanocube and nanorod populations, lab L6, Sample 1.

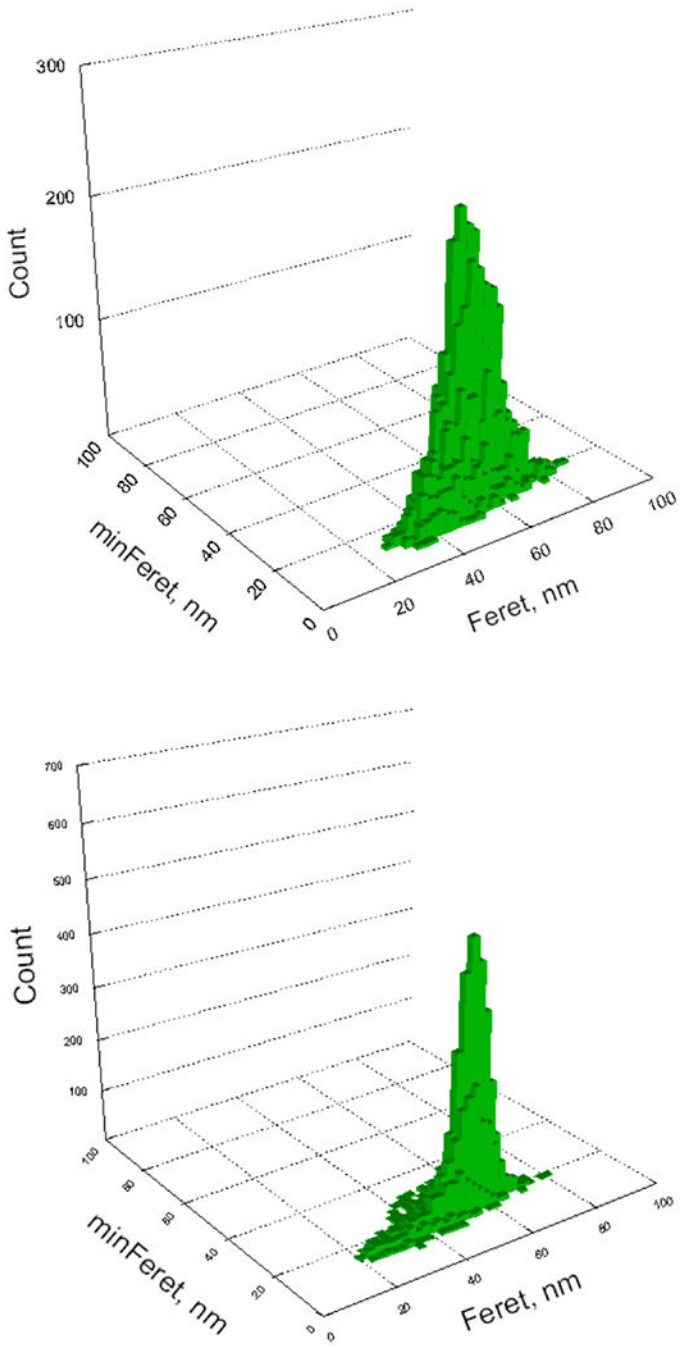

Figure 12.
Feret/minFeret bivariate plots; top = Sample 1, bottom = Sample 2, lab L6.

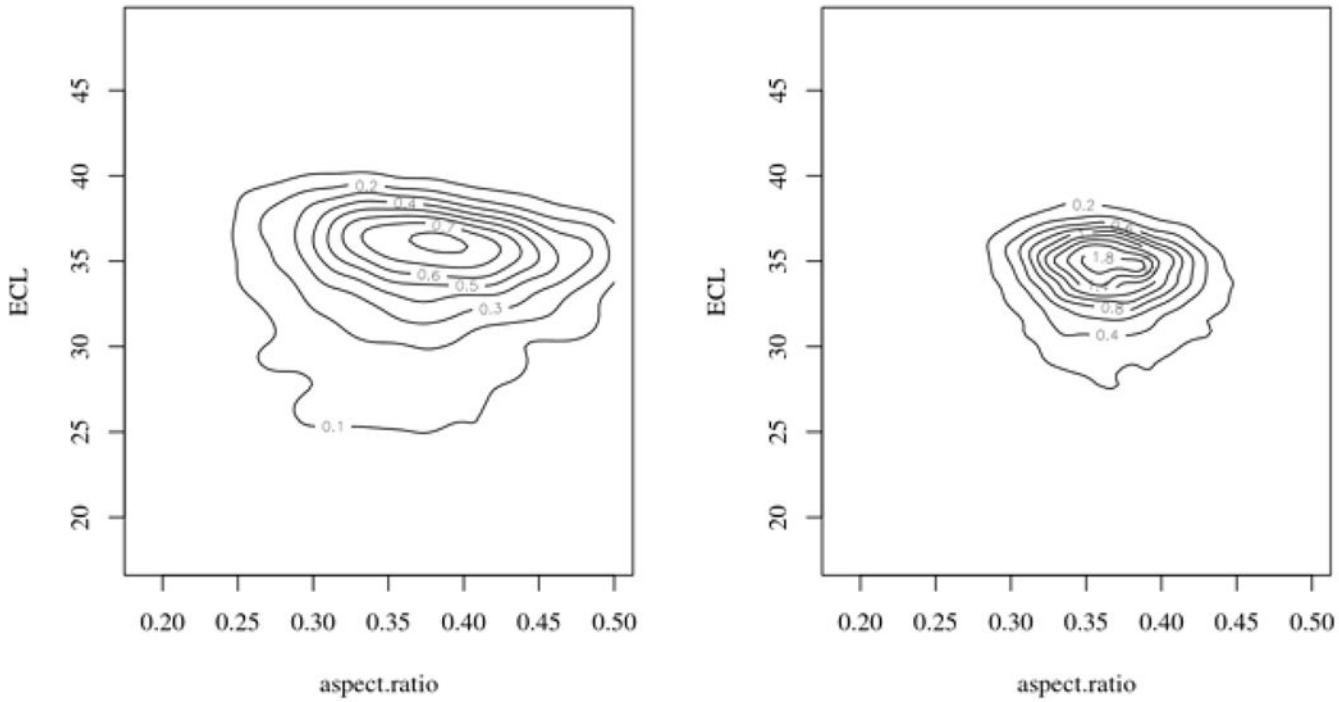

Figure 13.
ECL versus aspect ratio, lab L6. Sample 1 on the left, Sample 2 on the right.

Table 1.

Instrument conditions for image acquisition, Lab L3.

Operating factor	Protocol detail
TEM instrument model	JEOL 1220
Operating mode (TEM, STEM)	TEM
Accelerating voltage	80 kV
Magnification	80k
Beam current	66 mA
Dates of analysis	2014 05 28; 2014 06 27; 2014 07 29

Table 2.

P-values of ANOVA comparison of descriptor means of Samples 1 and 2, labs L1–L5.

	***P*-values**	
Descriptor	**Scale**	**Width**
Feret	0.786	<0.001
minFeret	0.384	0.0188
Aspect ratio	0.096	<0.001
Compactness	0.776	<0.001

Table 3.

Coefficients of variation and uncertainties for Feret, minFeret, and aspect ratio scale and width parameters.

	Feret diameter (nm)				minFeret diameter (nm)				Aspect ratio (nm)			
	Sample 1		Sample 2		Sample 1		Sample 2		Sample 1		Sample 2	
Lab	**Scale**	**Width**	**Scale**	**Width**	**Scale**	**Width**	**Scale**	**Width**	**Scale**	**Width**	**Scale**	**Width**
L1	58.2	6.88	58.0	5.08	20.9	2.1	20.0	1.67	0.362	0.0611	0.343	0.0391
L2	53.5	6.56	53.6	4.79	19.1	2.2	17.7	2.01	0.356	0.0622	0.330	0.0392
L3L	53.1	6.90	54.5	5.36	20.5	2.3	19.4	2.07	0.388	0.0647	0.355	0.0398
L3U	53.1	7.14	54.6	5.15	21.1	2.4	20.7	2.24	0.402	0.0644	0.384	0.0414
L4	51.7	7.32	53.8	5.28	17.9	2.5	17.7	2.29	0.347	0.0655	0.330	0.0424
L5	64.4	7.91	63.6	5.71	23.2	2.9	22.1	2.16	0.361	0.0622	0.343	0.0412
L6	56.0	8.05	56.1	5.47	20.8	3.3	20.4	1.90	0.371	0.0649	0.367	0.0406
Grand average	55.7	7.25	56.3	5.26	20	2.53	19.7	2.05	0.369	0.0636	0.350	0.0405
Grand standard deviation	4.40	0.552	3.56	0.294	1.67	0.412	1.60	0.213	0.0191	0.0017	0.020	0.0012
C_v, %	7.91%	7.61%	6.32%	5.6%	8.14%	16.3%	8.11%	10.4%	5.17%	2.67%	5.70%	3.03%
U_{ILC}, %	16.9%	16.3%	13.5%	12.0%	17.4%	34.9%	17.3%	22.3%	11.1%	5.71%	12.2%	6.48%

Table 4.

Comparison of measurement uncertainties for descriptor scale and width grand means: gold nanospheres (Rice et al 2013) and gold nanorods. S1 = Sample 1; S2 = Sample 2.

Sample and descriptor	Scale	Width	Width/scale
Gold nanospheres			
ECD, nm	27.6	2.44	8.84%
U_{ILC}	5.54%	31.4%	
Gold nanorods			
S1 Feret, nm	55.7	7.25	13.0%
U_{ILC}	16.9%	16.3%	
S1 aspect ratio	0.369	0.0636	17.2%
U_{ILC}	5.17%	2.67%	
S2 Feret, nm	56.3	5.26	9.34%
U_{ILC}	13.5%	12.0%	
S2 aspect ratio	0.350	0.0405	11.6%
U_{ILC}	5.70%	3.03%	